Received: 21 November 2019 | Revised: 22 September 2020 | Accepted: 25 September 2020

DOI: 10.1111/geb.13209

RESEARCH PAPER

Global Ecology and Biogeography A Journal of Macroecology WILEY

Climate-induced variation in the demography of 14 tree species is not sufficient to explain their distribution in eastern North America

Amaël Le Squin[1] | Isabelle Boulangeat[2] | Dominique Gravel[1]

[1]Biologie, Université de Sherbrooke, Sherbrooke, QC, Canada

[2]Inrae Centre de Lyon-Grenoble, LESSEM Saint Martin d'Heres, Rhône-Alpes, France

Correspondence
Amaël Le Squin, Université de Sherbrooke, département de Biologie, 2500 Boulevard de l'Université, Sherbrooke (Québec) J1K 2R1, Canada
Email: amael.lesquin@gmail.com

Funding information
Natural Sciences and Engineering Research Council of Canada, Grant/Award Number: Strategic grant

Editor: Benjamin Blonder

Abstract

Aim: Dynamic range models are proposed to investigate species distributions and to project range shifts under climate change. They are based upon the Hutchinsonian niche theory, specifying that the occurrence of a species in an environmental space should be limited to positions where the intrinsic growth rate is positive. Evaluating population growth rate is, however, difficult for physiologically structured populations, such as forest stands, owing to size-induced individual variation in performance. Therefore, we still have a limited understanding of which aspect of tree demography contributes the most to their geographical range limit. We develop an index of demographic performance for size-structured populations and study its variation across a climatic gradient. We then investigate the relationship between the demographic performance index and species distribution.

Location: North America (57–124° W, 26–52° N).

Time period: 1963–2010.

Major taxa studied: Fourteen tree species.

Methods: We represent forest dynamics with a size-structured population model and neighbourhood competition with the perfect plasticity approximation. We then derive the lifetime reproduction per individual, R_0, in the absence of density dependence. Using forest inventory data, we assess how tree demography for each species varies with climate. We test the model by comparing R_0 and the probability of occurrence within species ranges.

Results: We find that both growth and mortality rates vary across species distributions, but climate explains little of the observed variation. Individual size and neighbourhood competition are the primary explanatory variables of tree demography. Finally, we find that R_0 relates weakly to the probability of occurrence, with no systematic decline in population growth rates towards the range limits.

Main conclusions: Spatial and size-induced variation in tree growth and mortality do not explain range limits and are insufficient to enable an understanding of tree dynamics. We propose that phenomena perceived mostly at the metapopulation scale should also be considered.

KEYWORDS
climate, competition, demography, niche theory, population growth rate, range shift, species distribution, structured-population model, scaling up

1 | INTRODUCTION

A common, but rarely tested, assumption in ecology is that a species is more likely to be found in a location where it performs the best. Indeed, the probability of occurrence across a species range should be correlated positively with its per capita intrinsic growth rate (McGill, 2012). Hutchinsonian niche theory (Hutchinson, 1957; Maguire, 1973) posits that species are limited to locations where environmental conditions (i.e., properties external to the organism) allow a population to persist. This hypothesis is at the core of species distribution models and can be used to identify climatic variables constraining species ranges, whilst their projection into the future can forecast potential range shifts.

The most concise formulation of this niche theory relates population growth rate, r, to the species niche: the hypervolume formed by the environmental factors space is the set, such that $r \geq 0$ (Holt, 2009; Godsoe et al., 2017). Formally, let $r_i(\mathbf{E}, \mathbf{R})$ be the growth rate of a focal species, i, when rare, viz. the intrinsic growth rate for a given environment, $\mathbf{E}$, and quantity of resources, $\mathbf{R}$. The equation $r_i(\mathbf{E}, \mathbf{R}) \geq 0$ specifies that the fundamental niche corresponds to locations where $\mathbf{E}$ and $\mathbf{R}$ allow positive growth. An equivalent representation is the lifetime number of recruits per individual, which is traditionally denoted by $R_{0,i}$ (de Roos, 1997; Pulliam, 2000), where i is still the species index. A sustainable population requires that $R_{0,i}(\mathbf{E}, \mathbf{R}) \geq 1$, whereby an individual must at least replace itself over its life span. This definition of niche allows species i to influence the rates of other species within the community, while responding to feedbacks on its own demographic rates. Hereafter, we drop index i, but it is important to remember that $R_{0,i}$ is a species-specific rate related to species i.

Difficulties in testing niche theory are rooted, in part, in the challenge of measuring population growth rates (McGill, 2012), especially for physiologically structured populations (Diekmann et al., 1990). For instance, the age or size of an individual influences its reproduction success, feeding behaviour and probability of death. When combined with density dependences and environmental influences, these age and size structures might blur the relationship between the occurrence of a species and its variations in R_0 along an environmental gradient. Nevertheless, individual-based structured-population models can bring insight to addressing the complexity of population dynamics. Such models, however, are demanding in terms of their parameterisation, and they are difficult to analyse. Good examples are forest trees, which can be modelled by spatially explicit simulators that account for single-tree development and the availability of light to an individual (e.g., Pacala et al.., 1993). These forest simulators focus upon the individual level, which is the scale relevant for studying competition and climate responses. Nonetheless, interesting questions typically relating to biogeography (including tree species distributions) lie at the population level, that is to say, with R_0.

The relationship between tree species ranges and population growth has recently come under scrutiny, both in Europe (Thuiller et al., 2014) and in north-eastern North America (McGill, 2012). Little correspondence has been found between r and tree species distributions owing to uncertainty that is associated with demographic parameters (Thuiller et al., 2014). Even negative correlations were found, which challenges the common assumption that a species is most abundant in its optimal environment (McGill, 2012). The inclusive niche was proposed as an alternative explanation to these negative correlations. Here, weak competitors have their fundamental niche reduced to a smaller realised space, in a trade-off between competitive ability and environmental tolerance (Serrano et al., 2015). Therefore, weak competitors can be more abundant in suboptimal environments.

Dynamic range models (DRMs) have been developed recently to get closer to individual demographic rates, while scaling up to the population level (Pagel & Schurr, 2012). Dynamic range models are hierarchical statistical models that relate species abundances to environmental data using two latent variables: population growth rate (r) and dispersal. These models can also track uncertainties in the data that arise at the demographic level, biogeographical level and observer level.

Currently, no standard method exists that would derive a single performance index from demographic rates (Purves, 2009). Thus, all studies linking species distributions to individual performance lie in the midst of "uncharted territory". Indeed, McGill (2012), Pagel and Schurr (2012) and Thuiller et al. (2014) have explored very different ways of linking distributions to population performance. Yet, they have all agreed that combining the three vital rates, namely, individual growth, mortality and fecundity, into r is difficult and that r itself cannot be derived easily from censuses. Building upon these papers, we derive r from a forest dynamics model that uses the three vital rates. In this paper, we focus exclusively on radial growth and mortality and make them life-stage dependent, which is of primary importance in propagating uncertainties up to r (Clark, 2003; λ in his article).

Our main objective in this study is to investigate whether the distribution of North American tree species is driven by the effect of climate and light competition on individual demography. The abundant-centre hypothesis postulates that demographic performance should decline towards range margins (Sagarin & Gaines, 2002). We therefore investigate two predictions: (i) that per capita growth rate should vary with climate; and, as a result, (ii) that per capita growth rate should decline at range margins where occurrence probabilities tend to zero. We represent forest stand dynamics by relating tree demography to evolving cohorts, thereby accounting for neighbourhood competition and ontogenetic variation in demography. This model relies on McKendrick–von Foerster

equations that link demography to cohort dynamics and is coupled with the perfect plasticity approximation (PPA) to describe neighbourhood competition (Strigul et al., 2008). We derive a formula from the McKendrick–von Foerster equations to combine individual tree growth, mortality and fecundity rates into R_0, which is the per capita growth rate. We then evaluate how components of tree demography (individual growth and mortality) respond to climate, individual size and competition. We expect an optimal climate for each species within the middle of its range, with better performance in light than shaded conditions. Thereafter, we test whether R_0 is positively correlated with the probability of occurrence and whether it declines towards range limits. The analysis is performed for the 14 most abundant tree species that are native to eastern North America.

2 | THE MODEL

2.1 | Model structure

We model forest dynamics using a physiologically structured population model (PSPM), which we have made spatially explicit, based on the study by Strigul et al. (2008). A physiologically structured model distinguishes individuals that are at different stages of development. We first provide general definitions that are related to PSPMs and then describe our own. PSPMs are based upon individual states (hereafter, *i*-states). The *i*-states are collections of variables exhibiting the following two properties (de Roos, 1997, for an overview of PSPMs):

1. The *i*-states completely determine the growth rate, death rate and birth rate of individuals at any given time (possibly together with the present environmental state), and its influence on the environment.
2. Future values of *i*-states are completely determined by their present values, together with the intervening environmental history as encountered by the individual of concern.

The environment is accounted for by the environmental state (hereafter, *e*-state). Formally, an *e*-state is a collection of biotic and abiotic factors that characterise the environment in which an individual lives and that affect individual performance. In this paper, we consider two kinds of *e*-states: (i) feedback loops, which both influence and are influenced by individuals of all species; and (ii) external forcing factors, which are imposed on the population. By definition, the former requires a dynamic description. We ignore random variation among individuals that are in the same *i*-state and which experience the same *e*-state. The model subsequently represents cohorts rather than individual trees.

Cohort dynamics of species j and diameter s and that are located in x are modelled by a spatially explicit version of the von Foerster–perfect plasticity approximation model (Strigul et al., 2008; hereafter, von Foerster–PPA):

$$\frac{\partial N_j(s,x,t)}{\partial t} = -\frac{\partial G_j(s,x;s^*(x,t))\,N_j(s,x,t)}{\partial s} - \mu_j(s,x;s^*(x,t))\,N_j(s,x,t) \quad (1)$$

$$N_j(0,x,t) = \frac{1}{G_j(0,x;s^*(x,t))}\int_0^\infty N_j(s,x,t)\,F_j(s;s^*(x,t))\,ds \quad (2)$$

where N_j is the number of trees of species j per unit size per unit space (it is a density, and only $\iint Ndsdx$ can be considered as a number of individuals); G is the growth rate of individuals, μ is the mortality rate, and F is the effective fecundity function (for a list of notations, definitions and units for each variable and parameter, see Table 1). Although we developed the model with a dispersal kernel, we decided to use a δ-Dirac distribution in this paper to maintain model tractability. Therefore, dispersion is localised to patch x and does not appear in Equation (2). The three demographic rates are affected by a size threshold, S^*, which is a feedback loop that is defined formally below. External factors (at a location x) influence only G and μ. Equation (1) describes cohort demography, whereas Equation (2) describes recruitment. Together, Equations (1) and (2) represent the structured-population dynamics of trees. We use tree diameter at breast height (d.b.h.) as a single *i*-state, and we use allometric functions from Purves et al. (2007) to compute tree height and crown diameter.

Recent studies have extended the von Foerster–PPA model to include either nitrogen or water competition (Dybzinski et al., 2011; Farrior et al., 2013). Although plants are likely to experience co-limitation of resources (e.g., light, moisture, nitrogen) both intra-annually and across their life spans, leaf and root growth rates can be dominated by limitation of one particular resource at any given point in time. Yet, the identity of the limiting resource is dynamic and will shift throughout the growing season and throughout the development of an individual plant within a forest stand (Farrior et al., 2013). Thus, modelling water and nutrient dynamics remains a challenge, as would be the case for parameterisation of demographic rates. We limit the feedback loop solely to competition for light, which is the major driver of forest dynamics in north-eastern North American forests, especially for saplings (Kobe, 2006; Pacala et al., 1996; Purves et al., 2007). To compensate for the lack of moisture competition, we base the *e*-states on precipitation variables and temperature, which affects metabolic rates (Brown et al., 2004) and, therefore, water demand. Nutrients are not explicitly considered as *e*-states, but their effects upon radial growth and mortality are captured, in part, by random effects.

Competition for light is represented by a critical height that partitions the forest into the understorey and the overstorey (Figure 1). The vertical position of trees determines growth and mortality thereafter. The equation describing the feedback loop between cohort dynamics and light availability is:

$$1 = \sum_{j=1}^{n}\int_{s^*(x)}^{\infty} N_j(s,x,t)\,\mathscr{A}_j(s;s^*(x,t))\,ds \quad (3)$$

where $\mathscr{A}$ denotes the cross-sectional area of the crown of an individual of size s (Figure 1). Equation (3) defines a size threshold, s^*,

TABLE 1 Notations used in this paper (sorted alphabetically using roman equivalents of the greek letters)

Symbol	Definition	Unit
$\mathscr{A}$	Area of the cross-section of the crown	a
age_{max}	Maximum age from Burns (1990a, 1990b)	T
dbh_{max}	Maximum *dbh* from Burns (1990a, 1990b)	ℓ
$\mathscr{F}$	Number of seeds per tree's crown area per time	$a^{-1}T^{-1}$
F	Effective fecundity function, *i.e.*, number of germinating seeds	T^{-1}
F_{Purves}	Effective fecundity function (Purves et al., 2008)	T^{-1}
G	Growth of individuals	ℓT^{-1}
μ	Mortality rate, $\mu = -\log(1-\text{p})$, where p is the annual probability of mortality	T^{-1}
N	"Density" of trees	$\ell^{-1}a^{-1}$
$\nabla\tilde{\rho}$	Vector field of $\tilde{\rho}_0$	∂_x, ∂_y
Ω	Landscape or expert map, $\Omega \subseteq R^2$	a
φ	Ratio of ΔAIC_c for models with VIF < 20	–
R_0	Net population growth rate	–
ρ_0	Net population growth rate using F_{Purves} and s^x_∞	–
$\tilde{\rho}_0$	Standardised ρ_0	–
s	Size of individuals (either d.b.h. or height)	ℓ
s^*	Size threshold that separates the forest into two strata	ℓ
s^*_c	Constant size threshold, value set to 0 m or 10 m for the maps	ℓ
s^x_{max}	Maximal d.b.h. that a tree would have at location x without competition	ℓ
s^x_∞	Integral's upper bound in ρ_0 formula	ℓ
t	Time	T
x	Space variable, $x \in \Omega$	–

Note: T stands for time unit, ℓ is individual tree length unit, and a is the spatial unit which is a length if the forest is one-dimensional, and an area, if it is a two-dimensional forest.

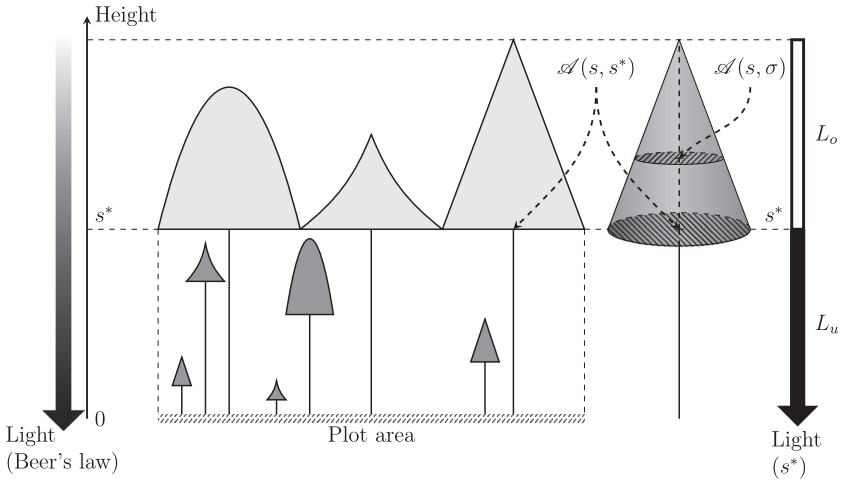

FIGURE 1 Traditionally, light availability is assumed to decrease progressively from the top of the canopy to the forest floor, obeying Beer's law (left arrow). Here, we assume that there is a threshold, s^*, that partitions the forest into two strata, thereby defining two light levels (right arrow): L_u and L_o for understorey and overstorey light, respectively. Therefore, light is a stepwise function of canopy height. The threshold, s^*, is the maximum height at which the canopy is closed; at this particular height, the sum of all the cross-sections equals the plot area. $\mathscr{A}(s, \sigma)$ is the crown cross-sectional area at height σ for an individual of height s

which differentiates the behaviour of individuals that are above s^* from those that are below; hence, s^* is such that the sum of the area of individual crowns equals the area of the plot being considered. Trees with a height below s^* are fully shaded, whereas trees above s^* are in the overstorey and receive direct sunlight. When the canopy is open, a positive value of s^* cannot be attained and therefore s^* is set to zero.

When the size variable is the height of trees, s^* is independent of the species. However, when the d.b.h. is the size variable, s^* becomes species specific (owing to species specificity of the allometric functions relating height to d.b.h.). It is noteworthy that the dynamics of s^* depend upon all species dynamics; therefore, s^* includes both intra- and interspecific competition. Equation (3) is adapted from Strigul et al. (2008) and therefore obeys the PPA assumption: the canopy is a collection of small crowns that can be reorganised such that the area occupied is maximised. Despite this optimisation of sun exposure being considered theoretical, combining PPA with von Foerster equations can accurately reproduce forest dynamics at stand scales, within a relatively homogeneous physical environment (Purves et al., 2008; Strigul et al., 2008). The set of three equations (Equations 1–3) forms a tractable PSPM, which allows us to derive R_0 analytically.

2.2 | Net reproduction rate R_0

Henceforth, the height s^* that separates shaded trees from sun-exposed trees is referred to as "competition". We used the method of characteristics (Olver, 2014) to calculate the net reproduction rate at a location, x, within a landscape, Ω, as a function of a constant competition s_c^*. This mathematical technique is used to solve certain partial-differential equations, as commonly used in transport equations. For example, Equation (1) describes the advection (bulk motion) of trees growing at a non-constant speed, G, along the size axis (which is either height or diameter). Characteristics allow us to follow individuals throughout their life span (i.e., they represent the trajectories of individuals in the time–size plane; for an example, see Supporting Information Appendix S1, Figure S1.1). The derivation of R_0 is detailed in the Supporting Information (Appendix S1). Three underlying assumptions are made for this calculation: (i) s^* is considered fixed and known at a value s_c^*; (ii) only trees larger than s_c^* can reproduce (Strigul et al., 2008); and (iii) dispersal is limited to the patch, as stated by Equation (2). Subsequently, the net reproduction rate in a patch, x, is consequently:

$$R_0\left(x, s_c^*\right) = \exp\left[-\int_0^{s_c^*} \frac{\mu\left(s, s_c^*, x\right)}{G\left(s, s_c^*, x\right)} ds\right] \times \int_{s_c^*}^{\infty} \frac{F\left(s, s_c^*\right)}{G\left(s, s_c^*, x\right)} \exp\left[-\int_{s_c^*}^{s} \frac{\mu\left(\sigma, s_c^*, x\right)}{G\left(\sigma, s_c^*, x\right)} d\sigma\right] ds. \quad (4)$$

Equation (4) can be divided into two biological processes:

1. $\exp\left[-\int_0^{s_c^*} \frac{\mu(s, s_c^*, x)}{G(s, s_c^*, x)} ds\right]$ is the proportion of individuals that survive up to the canopy of height s_c^* in plot x, and
2. $\int_{s_c^*}^{\infty} \frac{F(s, s_c^*)}{G(s, s_c^*, x)} \exp\left[-\int_{s_c^*}^{s} \frac{\mu(\sigma, s_c^*, x)}{G(\sigma, s_c^*, x)} d\sigma\right] ds$ is the expected production of offspring for an individual that is located in x, during its life span. It has two subterms:

2.1. $\frac{F(s, s_c^*)}{G(s, s_c^*, x)}$ is the number of offspring per unit time for individuals that grow at speed G, and

2.2. $\exp\left[-\int_{s_c^*}^{s} \frac{\mu(\sigma, s_c^*, x)}{G(\sigma, s_c^*, x)} d\sigma\right]$ is the survivorship of trees of size s. Given that μ and G are both positive functions, survivorship is a decreasing function of s.

From Equation (4), we understand that the reproduction rate, R_0, can be increased by reducing the competition, s_c^*, by accelerating the average understorey growth, $G(s < s_c^*)$, by diminishing the average mortality rate, μ, or by enhancing the fecundity, F. The mathematical proofs for these three mechanisms are provided in the Supporting Information (Appendix S1). Equation (4) is a generalisation of the R_0 that was derived by Purves but was limited to open canopies and stepwise demographic functions. We expressed R_0 for any individual growth, mortality or overstorey fecundity functions and for any canopy height. The same three assertions can be drawn from his study (Supporting Information Appendix S1); however, contrary to Purves, we cannot assert that a faster average overstorey growth rate leads to an increase in R_0 (owing to the complexity of the computations). For the same reason, we cannot calculate the value of s_c^* for a population at equilibrium (i.e., when $R_0 = 1$), except when the demographic rates are easier to compute, as step functions (Purves, 2009, Supporting Information Appendix S1 for the proof).

The R_0 represents the number of individuals produced by a species when rare and that does not affect a community at equilibrium. A species can invade a forest stand with a steady canopy height, s_c^*, whenever $R_0 > 1$. It is, by definition, computed on the linearised problem, which does not consider density dependences (Diekmann et al., 1990).

2.3 | Data

We parameterised the demographic functions G (individual growth) and μ (mortality) using data that were obtained from permanent sample plots of the Forest Inventory and Analysis (FIA, US Department of Agriculture Forest Service), the Ministère des Forêts, de la Faune et des Parcs du Québec, the Ministry of Natural Resources and Forestry of Ontario, the Ministry of Natural Resources of New Brunswick, and the forest products company Domtar (for a map of the data, see Supporting Information Appendix S2, Figure S2.2). After removal of plots that experienced fire or logging, there were 7,704,442 individual measurements (106 species distributed among 132,240 plots). A record consists of the tree identity, the species, the year in which the individual was measured, the d.b.h., the latitude and longitude of the plot, and the status of tree (alive or dead). Measurements occurred between 1963 and 2010, and frequencies of measurement range from once a year to once every 40 years (with 96% of the data between once every three and once every 15 years). Both radial growth and mortality are highly variable across the distributions of the individuals (Supporting Information Appendix S2).

Climate data were extracted for each plot using ANUSPLIN software (McKenney et al., 2011) based upon the latitudinal and longitudinal coordinates of the permanent plots. Note that for privacy reasons, the FIA offsets plot locations ≤1.6 km (Gray et al., 2012), which might result in mismatches between the real climate of the plot and the climate that we assigned. We selected 19 climatic variables (Supporting Information Appendix S2) covering the period

1958–2010 with a spatial resolution of 60 arc s (*c.* 2 km^2). To account for climate variability before each tree measurement, we averaged each temperature and precipitation variable over a 5-year period using a moving average (5 years is the most frequent interval among measurements that are included in the database, with 38.8% of observations).

We calculated individual tree height and crown area from allometric functions and parameters that are provided by Purves et al. (2007). We considered the d.b.h. of all trees, although most Canadian inventories start with individuals having diameters >100 mm, whereas USA inventories start at 127 mm (5 inches). Some trees have been recorded as dead and then alive; we considered the last living state to be true and ignored "resurrection" events in estimation of mortality. By definition, growth and mortality rates require at least two measurements from an individual tree. After calculating the threshold, s^*, in each plot (for the algorithm, see Supporting Information Appendix S2; and for the R code, see the Data Availability Statement), trees measured once were discarded. For the growth analysis, we eliminated dead trees and individuals that had either a non-positive d.b.h. increment or radial growth >25 mm/year. We parameterised the model for the 14 most abundant species in north-eastern North America (Supporting Information Appendix S2), but we considered all 106 species in the database for the computation of s^*. The 14-species dataset that is used in this paper contains 69,954 plots (75% in the USA and 25% in Canada), for a total of 3,816,854 individual measurements. *Abies balsamea* is the most frequently measured species, with 822,265 individual measurements, whereas *Tsuga canadensis* is the least frequently measured, with 66,008 individual measurements. The climatic and geographical ranges of each species can be found in the Supporting Information (Appendix S2).

2.4 | Parameterisation of demographic rate functions

We used linear mixed models to parameterise the individual growth (G) and mortality (μ) rates as a function of climate, canopy status (understorey, if below s^*; overstorey, if otherwise) and size (d.b.h.). For the fecundity, we used the functions and values from the study by Purves et al. (2008). We tested linear and quadratic functional forms for the temperature, precipitation and d.b.h. effects, which were all standardised using normal scores. To obtain an optimal climate in the quadratic case, it was necessary to have a negative (positive) slope preceding the squared climate variables for the growth (mortality). Constraining the parameters would force the optimal climate to be contained within the data that were used for parameterisation; therefore, we did not set any constraints. The 19 variables for temperature and precipitation allowed us to try different combinations; however, we preselected certain climatic assemblages based upon the interpretability of the models and the literature (Supporting Information Appendix S3). Each set of species-specific demographic parameters was estimated separately. We based the model comparison on information criteria and R^2 (both marginal and conditional R^2 were estimated with the package *MuMIn*; Barton, 2019). We ranked the models for each species and selected the model that, on average, fitted the best according to information criteria. This model was then imposed on the 14 species. R scripts that were used to format the data and to estimate demographic parameters are available on Github (see Data Availability Statement).

2.4.1 | Growth

For the individual growth rate, we assumed a lognormal distribution; thus, $\log(G)$ is normally distributed. We normalised the logarithm of growth as:

$$Y_G = \frac{\log(G) - E\left[\log(G)\right]}{SD\left[\log(G)\right]},$$

and implemented the following generic model:

$$\begin{aligned} E\left[Y_G^{ij}\right] &= \beta^{(0)}_{j,(x,t)[i]} + \beta_j^{(1)}\text{canopy status} \\ &+ \left(\beta_j^{(2)} + b_j^{(2)}\text{canopy status}\right) T + \left(\beta_j^{(3)} + b_j^{(3)}\text{canopy status}\right) T^2 \\ &+ \left(\beta_j^{(4)} + b_j^{(4)}\text{canopy status}\right) P + \left(\beta_j^{(5)} + b_j^{(5)}\text{canopy status}\right) P^2 \\ &+ \left(\beta_j^{(6)} + b_j^{(6,1)}T + b_j^{(6,2)}T^2 + b_j^{(6,3)}P + b_j^{(6,4)}P^2\right)\text{d. b. h.} \\ &+ \left(\beta_j^{(7)} + b_j^{(7,1)}T + b_j^{(7,2)}T^2 + b_j^{(7,3)}P + b_j^{(7,4)}P^2\right)\text{d. b. h.}^2 \end{aligned} \quad (5)$$

where $E\left[Y_G\right]$ is the expected value of the normalised logarithm of growth, and T and P are the associated explanatory temperature and precipitation, respectively. Canopy status is Boolean (true for the canopy trees, and false otherwise). The indices i and j denote the individual and species, respectively, and $(x, t)\,[i]$ index denotes the group effects (plot x and year t of the ith individual). Random effects (with a maximum of three effects: spatial, temporal and plot-specific temporal, respectively) are normally distributed as:

$$\beta_j^{(0,x)} : \mathcal{N}(0, \boldsymbol{\sigma}_x^{\text{growth}})$$

$$\beta_j^{(0,t)} : \mathcal{N}\left(0, \boldsymbol{\sigma}_t^{\text{growth}}\right)$$

$$\beta_j^{(0,xt)} : \mathcal{N}\left(0, \boldsymbol{\sigma}_{xt}^{\text{growth}}\right)$$

Mixed models allow us to group individuals by plots and the years of the second measurement, allowing us to consider spatial and temporal structures. The plot effect incorporates variation that is driven by local factors, such as soil conditions and disturbance history, whereas the year (within plot identity) represents temporal variation that is not included in climate. The values of β are the regression coefficients, and the values of b correspond to different variable interactions. Climate interacts with the crowding effect (canopy status) to account for climate response variation to the neighbourhood of the individual. Lastly, as bigger trees might be

favoured or disadvantaged by climate, d.b.h. interacts with climatic variables *T* and *P*.

We used the package *lme4* (Bates et al., 2015) to estimate the parameters (values of β and *b*). We tested sub-models of Equation (5) to evaluate the effects of competition and climate on *G*. We used a top-down strategy to select first the random effect structure and, second, the fixed structure. We compared models with the corrected Akaike information criterion (AIC_c), but retained models with a maximum variance inflation factor (VIF) that was <20 to avoid correlations between variables (Zuur et al., 2010). We chose a VIF of 20 because of one model for growth that has reasonable maximum VIFs (<6) for 11 species, and three species where VIF > 6, with 19 as a maximum for *Fagus grandifolia*. We judged that a VIF of >20 implies too much collinearity (F. Guillaume Blanchet, personal communication, December 2018). We denote ΔAIC_c as the difference between a model *i* and the model having the smallest AIC_c:

$$\Delta AIC_c = AIC_c^{(i)} - AIC_c^{(min)}$$

The best model has the lowest AIC_c or, equivalently, $\Delta AIC_c = 0$. Calculation of ΔAIC_c was unconstrained with respect to the best model; yet, owing to the VIF constraint, the selected model is not the model with $\Delta AIC_c = 0$. We exclusively used models satisfying the constraint VIF < 20, from which we computed the common logarithm of the ratio between the ΔAIC_c of each model and the minimum ΔAIC_c:

$$\varphi = \log_{10}\left[\frac{\Delta AIC_c}{min\left(\Delta AIC_c\right)}\right] \quad (6)$$

This ratio represents, within the subset of models satisfying the constraint VIF < 20, how many times (to a power of 10) the best model compares to the other models. The common logarithm provides a convenient scale for comparing the models. The best constrained model has $\varphi = \log_{10}(1) = 0$.

2.4.2 | Mortality

For the mortality rate, the response variable, *Y*, is a Boolean describing the transition state between two records (true, if there is a transition from alive to dead; false, if the individual remains alive). The observation of a mortality event depends on the survey interval, Δt (Lines et al., 2010). To survive from t_0 to $t_1 = t_0 + \Delta t$, an individual, *i*, must survive each year, according to:

$$P\left[\text{survival } i\text{: } t_0 \rightarrow t_1\right] = 1 - \left(1 - P\left[\text{annual mortality } i\right]\right)^{\Delta t}$$

where *P* stands for probability. Thus, the probability of observing a mortality event within a span, Δt, is:

$$P\left[\text{mortality } i\text{: } t_0 \rightarrow t_1\right] = 1 - \left(1 - P\left[\text{annual mortality } i\right]\right)^{\Delta t}$$

We assumed that *Y* follows a binomial distribution and used the complementary log–log link function, *g*, to account for the time between two surveys (offset on the intercept; for a short description of the complementary log–log function, see Supporting Information Appendix S3):

$$g\left(E\left[Y_\mu^{i,j}\right]\right) = \log\left\{-\log\left(1 - E\left[Y_\mu^{i,j}\right]\right)\right\}$$

We worked with the following model:

$$\begin{aligned} g\left(E\left[Y_\mu^{i,j}\right]\right) &= \beta_j^{(0)} + \beta_j^{(1)}\text{canopy status} + \text{offset}\left[\log\left(\Delta t_i\right)\right] \\ &+ \left(\beta_j^{(2)} + b_j^{(2)}\text{canopy status}\right)T + \left(\beta_j^{(3)} + b_j^{(3)}\text{canopy status}\right)T^2 \\ &+ \left(\beta_j^{(4)} + b_j^{(4)}\text{canopy status}\right)P + \left(\beta_j^{(5)} + b_j^{(5)}\text{canopy status}\right)P^2 \\ &+ \beta_j^{(6)}\text{d. b. h.} + \beta_j^{(7)}\text{d. b. h.}^2 \end{aligned} \quad (7)$$

where the same notations as the growth model are used. We did not include any group effect, given that some plots have only one record for certain years and species, whereas other plots have recorded no dead trees, which was a problem that was also faced by Kunstler et al. (2020). To minimise the uncertainty of death events and to have enough measures per species per time interval, we limited the dataset to measurements with $\Delta t \in [5, 11]$ (74.9% of the mortality database). Given that the probability of transition from dead to dead is one, we kept records up to the first death event only (or all measurements, if there were no death events).

For mortality, none of the Generalised Linear Mixed Models (GLMMs) from the package *lme4* converged on a solution. We suspect that despite the amount of data, there is little information owing to the rarity of tree mortality. We therefore used the package *rstanarm* (Goodrich et al., 2018), which examines GLMMs in a Bayesian framework, and removed the climate–d.b.h. interactions. We used four Markov chains and 3,000 iterations for each chain. We retained the default priors of *rstanarm*, which are Gaussian distributions for the regression coefficients (β), and exponential distributions for the standard deviations. Parameter values that were used later in the analysis are the medians of the posterior distributions. We used the widely applicable information criterion (WAIC; Hooten & Hobbs, 2015, and references therein) to select the best model. The WAIC is based upon the posterior predictive distribution (the distribution to predict new data) and is valid for hierarchical models. However, it assumes that the data are independent given a set of parameters, which could be problematic for our spatial data. As was the case for radial growth, we compared WAICs on a common logarithmic scale:

$$\psi = \log_{10}\left(\Delta WAIC + 1\right) \quad (8)$$

The best model has $\Delta WAIC = 0$, which implies that ψ is also null for the best model. Although there are R^2 estimates for Bayesian regression models, they cannot be compared; the explained variance can only be interpreted in the context of a single model (Gelman et al., 2018). Hence, we based our choice exclusively on the WAIC.

We checked the convergence of the selected model for all parameters and species with the Gelman–Rubin statistic (Gelman & Rubin, 1992, R-hat diagnostic). Typically, a chain with an R-hat of >1.05 is considered non-convergent; at convergence, R-hat should be one.

2.4.3 | Fecundity

The forest inventory data have few records of trees with a d.b.h. < 10 cm; thus, we could not parameterise the fecundity function, $F(s, s^*)$. Instead, we used the fecundity function that was defined by Purves et al. (2008) and parameterised as:

$$F_{\text{Purves}}(s, s^*) = \mathscr{F} \times \mathscr{A}(s, s^*), \text{with} \mathscr{F} = 0.0071 \quad (9)$$

where $\mathscr{F}$ is the number of seeds produced per sun-exposed tree crown area per unit time (Table 1). In this case, we defined a new quantity, ρ_0, as the net reproduction rate, R_0, with the reproduction function, F_{Purves}. The notation R_0 is strictly reserved for the general case, where the fecundity function is not restricted to the function of Purves.

By definition, ρ_0 corresponds to the net reproduction rate when the fecundity function is independent of climate (i.e., spatially constant). Once ρ_0 is calculated across the landscape, Ω (using Equation 12 defined below), we can estimate a convenient normalised quantity as:

$$\tilde{\rho}_0(x, s^*) = \frac{\rho_0(x, s^*) - min_{x\in\Omega}\left[\rho_0(x, s^*)\right]}{max_{x\in\Omega}\left[\rho_0(x, s^*)\right] - min_{x\in\Omega}\left[\rho_0(x, s^*)\right]} \quad (10)$$

This cancels the value of $\mathscr{F}$, which was a difficult parameter to estimate in the study by Purves et al. (2008), and bounds $\tilde{\rho}_0$ between zero and one.

2.5 | Occurrence probability

We evaluated the correlation for each species between $\tilde{\rho}_0$ and the probability of occurrence, P_{occ}, which is derived from a random forest model (Liaw & Wiener, 2002, R package). This is a way of transforming discrete presence and absence data into probabilities, which are continuous data. It has been shown that random forests perform well in terms of predicting tree species distributions (Prasad et al., 2006). Using a continuous probability rather than presence–absence data can be useful in the case where climatic conditions are favourable but species are absent because of stochasticity and, alternatively, where species are present but should not occur.

We trained the algorithm with coordinates from the sample plot dataset, where at least one species was recorded. We assigned zero to each coordinates–species couple where there were no records for that species in (x, y) after 1996, and one otherwise. We set the random forest with 2,000 trees, and 12 predictors over 19 to be selected at each tree node. More trees add precision and bound the generalisation error (i.e., the true error of the population as opposed to the training error only), without overfitting the data (Prasad et al., 2006). The explanatory variables set contained 19 bioclimatic variables (for the variables, see Supporting Information Appendix S2; for the equation see Supporting Information Appendix S6). The performance of the random forest was evaluated with the R^2 from Tjur (2009), and later denoted as R^2_{Tjur}.

2.6 | Species performance maps

We downloaded an expert range map, Ω_j (Little, 1971; Prasad & Iverson, 2003), for each species, j, and calculated $\tilde{\rho}_0$ for each location within Ω_j for a climate averaged over 5 years (from 2006 to 2010) and a canopy height s^* of either 0 m (no competition) or 10 m (the average for the distribution of s^* across the database is 9.6 m). Hereafter, we drop the index j and use only Ω, although the expert range maps are species specific.

We investigated, within the box that bounds our data (map in Supporting Information Appendix S2, Figure S2.2), how $\tilde{\rho}_0$ relates to the orthodromic distance from the closest edge of the distribution that was defined by Little (1971), and mapped the variations in $\tilde{\rho}_0$. In order to avoid spatial extrapolations of the demographic rates, we decided to limit our study to the region of parameterisation (e.g., *Betula papyrifera* extends to Alaska). To evaluate the direction in which $\tilde{\rho}_0$ increases, we computed its vector field, $\nabla\tilde{\rho}_0$, on Ω using the algorithm of Ritter (1987). The vector field, $\nabla\tilde{\rho}_0$, provides at any location, $x \in \Omega$, the gradient of $\tilde{\rho}_0$, which is its local direction of increase. We then separated Ω into two regions, north and south with respect to the centroid of Ω, and we averaged the gradients for each region. If $\tilde{\rho}_0$ decreases towards range limits, then both gradients should point towards the centre of the distribution. Thus, the gradient of the northern region should point southwards, and the gradient of the southern region should point northwards.

We must integrate upwards to infinity to compute $\tilde{\rho}_0$ (see Equations 10 and 11), but we found numerically that the integral beyond a height of 45 m is negligible (because $lim_{s\to\infty} G(s) = 0$ and $\mu > 0$). To be closer to the real maximum d.b.h. and height of trees for a given location, $x \in \Omega$ (rather than arbitrarily setting a maximum height of 45 m), we determined the upper boundary s^x_∞ of the integral of $\tilde{\rho}_0$ in three steps:

1. We obtained the species-specific maximal age (age_{max}) and maximal d.b.h. (d.b.h._{max}) from Burns and Honkala (1990a, 1990b). The data are in the Supporting Information (Appendix S2).
2. We computed the d.b.h. that a tree would have at the location x with the associated climate, clim_x, if it were spending its entire life in the overstorey up to the maximal age (using the solver ODE45 from Matlab):

$$s^x_{max} = \int_0^{\text{age}_{max}} G^{(\text{overstorey})}\left[s(t), \text{clim}_x\right] dt.$$

3. We set the local "infinite d.b.h.":

$$s_{\infty}^{x} = min\left(\text{d.b.h.}_{max}, s_{max}^{x}\right) \tag{11}$$

and replaced ∞ in Equation (4) with s_{∞}^{x}. If $s_{\infty} < s_c^*$, which happens when trees cannot reach the canopy before reaching their maximum ages, we set R_0 to zero.

Therefore, Equation (4) combines Equations (4), (9) and (11) to measure species performance:

$$\rho_0\left(x, s_c^*\right) = \exp\left[-\int_0^{s_c^*} \frac{\mu\left(s, s_c^*, x\right)}{G\left(s, s_c^*, x\right)} ds\right] \times \int_{s_c^*}^{s_{\infty}^x} \frac{\mathcal{FA}\left(s, s_c^*\right)}{G\left(s, s_c^*, x\right)} \exp\left[-\int_{s_c^*}^{s} \frac{\mu\left(\sigma, s_c^*, x\right)}{G\left(\sigma, s_c^*, x\right)} d\sigma\right] ds, \tag{12}$$

from which we can derive $\tilde{\rho}_0$ (using Equation 10). Equation (12) accounts for spatial differences in the maximum d.b.h. that are not included in the radial growth model. Its major difference from Equation (4) is the upper boundary of the expected production of offspring (the second integral), which makes Equation (12) specific to the present study, whereas Equation (4) is a generalisation of Purves (2009).

2.7 | Roadmap

We first parameterised individual growth and mortality as functions of climate and competition for 14 northern North American trees. Competition refers to the canopy status (in either the understorey or the overstorey) and was calculated using allometric functions and Equation (3). We then computed the population growth rates, $\tilde{\rho}_0$, within each species range, Ω, to test the abundant-centre hypothesis, together with correlations between $\tilde{\rho}_0$ and species performance.

3 | RESULTS

3.1 | Competition and climate effects on individual growth and mortality

We found that individual growth and mortality were weakly related to climate, and that individual tree size and competition were the predominant drivers of their variation (Figure 3).

Individual tree growth was, regardless of species, best explained by annual mean temperature (T_a) and annual precipitation (P_a), together with the plot random effect, and year within plot. The conditional R_c^2 was much higher than the marginal R_m^2, indicating that the random structure and, more specifically, that local conditions dominated explanatory variables. According to the calculated ratio, φ (Equation 6), and R^2, climate explained little variation in individual tree growth compared with tree d.b.h. (Figure 3; Supporting Information Appendix S3).

Our analysis revealed that growth was higher in the overstorey for all species (Figure 2a). Moreover, we found that the response to overstorey competition corresponded to the shade tolerance: individual growth of shade-tolerant species was less responsive to canopy gaps than that of shade-intolerant species (Figure 2b; Supporting Information Appendix S3, Table S3.6).

For mortality, the best model for all the species included the lowest annual temperature (T_m) and the three contiguous driest months (P_d). Diameter at breast height, competition and climate best explained tree mortality when combined, but were equivalent when taken separately, which differed from growth (Figure 3). All the Markov chains converged, regardless of parameters and species (R-hat histogram in Supporting Information Appendix S4).

Mortality was greater in the understorey for all species, except for *Tsuga canadensis* and *Fagus grandifolia*. Low shade-tolerant species responded more negatively to competition than did highly tolerant species (Figure 2c,d).

There was considerable uncertainty in parameter estimates for both rates (Supporting Information Appendix S3). More specifically, the mortality functions of *Abies balsamea*, *Betula papyrifera*, *Fagus grandifolia*, *Picea rubens*, *Pinus strobus* and *Populus tremuloides* were bell shaped or flat curves, but they could be U-shaped responses (which is more likely to be expected; Lines et al., 2010) according to the posterior distributions of their regression coefficients. *Abies balsamea* and *Populus tremuloides* were the two exceptions, given that they compensated for their negative mortality response to d.b.h.^{2}, with steep slopes related to d.b.h. The effect of competition was significant for most species and interacted with temperature, whereas interactions between competition and precipitation were mostly non-significant for both vital rates (Supporting Information Appendix S4, and csv files online). Thus, the advantage of having greater access to water resources for large trees might be compensated by their higher moisture demands.

3.2 | Relationship of demography and competition to tree distribution

The $\tilde{\rho}_0$ in Equation (12) relates species-specific demographic functions, which were estimated in the previous section 3.1, to population performance. Demographic performance, $\tilde{\rho}_0$, varied significantly, but there was no systematic relationship across ranges (Figure 4; maps in Supporting Information Appendix S5).

If the abundant-centre hypothesis is to be confirmed, the vector fields, $\nabla\tilde{\rho}_0$ (white and red arrows on the maps and Figure 4), should point towards species centroids. On the one hand, $\tilde{\rho}_0$ of six species (*Acer saccharum*, *Acer rubrum*, *Picea glauca*, *Pinus strobus*, *Thuja occidentalis* and *Tsuga canadensis*) increased from south-east to north-west (Figure 5). On the other hand, it increased towards the south for five species (*Abies balsamea*, *Betula papyrifera*, *Picea mariana*, *Picea rubens* and *Populus tremuloides*). Except for *Picea mariana*, note that the four other species had a negative slope associated with

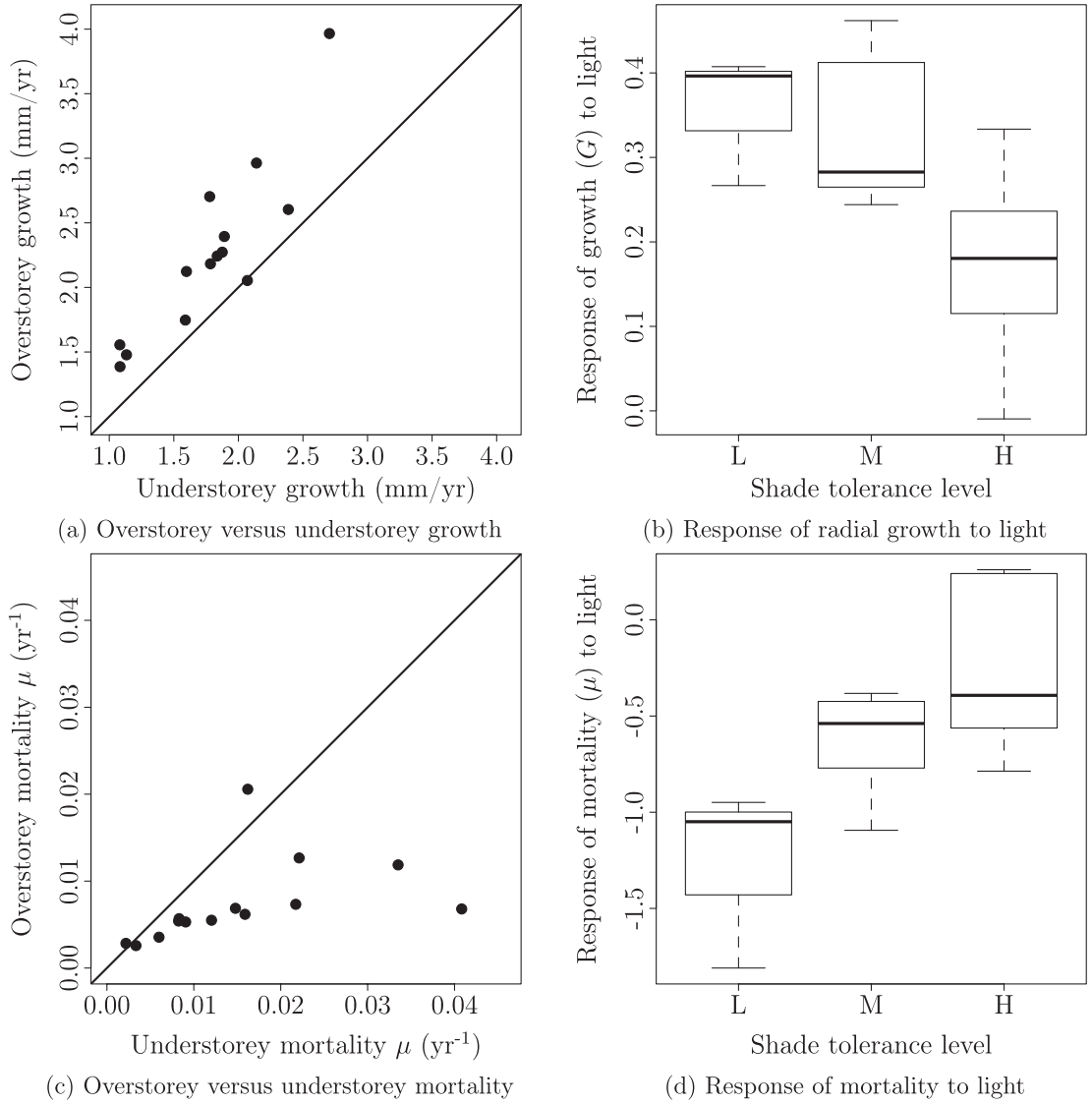

FIGURE 2 (a,c) Overstorey versus understorey growth and mortality of the 14 parameterised species for an averaged individual (i.e., all the explanatory variables of Equations (5) and (7) are set to their average values). The line is the identity function. (b,d) Response of species-specific radial growth, *G*, and mortality, μ, to light, grouped by three levels of shade tolerance: low (L), medium (M) and high (H). Growth of species reaching the canopy increases much more rapidly for shade-intolerant species than for tolerant ones, and the mortality decreases much more strongly for shade-intolerant species than for tolerant ones. For the parameters, see the Supporting Information (Appendix S3)

the quadratic d.b.h. term in the mortality model (parameter $\beta_j^{(7)}$ in Equation 7). The three remaining species (*Betula alleghaniensis*, *Fagus grandifolia* and *Picea banksiana*) did no exhibit a clear direction within their respective distribution, Ω. Correlations between $\tilde{\rho}_0$ and the orthodromic distance to the closest edge of Ω were negative for most species (Supporting Information Appendix S6), which corroborated that $\tilde{\rho}_0$ was not highest in the centre of species distributions, thereby challenging the abundant-centre hypothesis (Figure 5).

The lifetime number of recruits per individual, $\tilde{\rho}_0$, aggregates the three vital rates into a species-specific performance measure. We computed correlations between occurrence probabilities, P_{occ}, and individual growth and mortality to disentangle their effects upon $\tilde{\rho}_0$ (Supporting Information Appendix S6). Overall, we found no rule relating occurrence probabilities with demography. When P_{occ} was positively correlated with individual growth and negatively correlated with mortality, the correlation of P_{occ} with $\tilde{\rho}_0$ was also positive (e.g., *Betula papyrifera*; Supporting Information Appendix S6). In this case, correlations of P_{occ} with $\tilde{\rho}_0$ were consistently higher than correlations of P_{occ} with demography (Supporting Information Appendix S6, subsection S6.3). However, when P_{occ} was (counter-intuitively) positively correlated with mortality rates, the correlation of P_{occ} with $\tilde{\rho}_0$ dropped or even became negative (e.g., *Fagus grandifolia*; Supporting Information Appendix S6). These results demonstrate that there might be compensatory strategies (such as a higher recruitment rather than our constant fecundity function), which could explain why P_{occ} was positively correlated with mortality.

The correlation between $\tilde{\rho}_0$ and the probability of occurrence, P_{occ}, did not show any trend in the absence of competition (varying from −0.49 to 0.60), nor was there a trend with a canopy height of

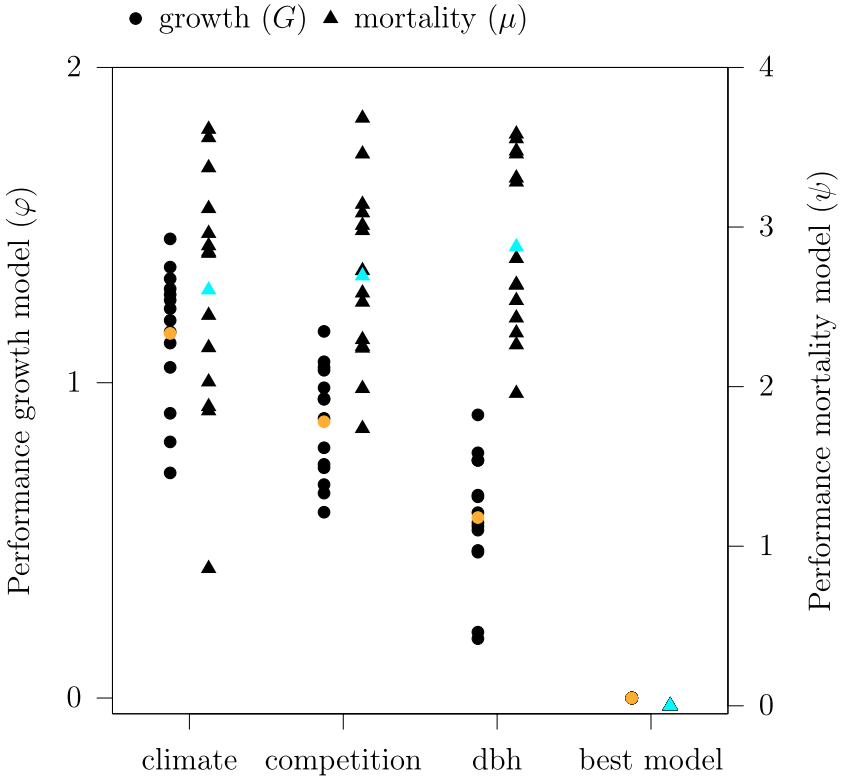

FIGURE 3 Performance, φ (growth, filled circles; Equation 6) and ψ (mortality, filled triangles; Equation 8), for four models (the closer to zero, the better). The black symbols represent the 14 species, and the coloured symbols are the average for each model. The model "climate" is the second-order polynomial containing T_a and P_a (growth) or T_m and P_d (mortality). The model "competition" includes only canopy status (*cs*) as a predictor, and the model "d.b.h." is the second-order polynomial containing d.b.h. The best model (written in an R-language style) for growth is $\text{growth} \sim 1 + (1|x) + (1|t) + (1|x{:}\ t) + (cs + \text{d.b.h.} + \text{d.b.h.}^2) * \left(T_a + T_a^2 + P_a + P_a^2\right)$. Mortality is best explained by $\text{mortality} \sim 1 + \text{offset}\left[\log(\Delta t)\right] + cs * \left(T_m + T_m^2 + P_d + P_d^2\right) + \text{d.b.h.} + \text{d.b.h.}^2$. All the tested models can be found in the Supporting Information (Appendix S3; Equations G2 and M7 are the best models for growth and mortality, respectively). All species have the same best model; thus, the black dots are hidden by the two coloured dots for the last column of this figure

10 m (ranges within −0.51 and 0.47). The correlation decreased with competition for most boreal species (*Betula papyrifera*, *Picea glauca*, *Picea mariana*, *Picea rubens*, *Pinus banksiana* and *Thuja occidentalis*, but not *Abies balsamea*). For the shade-intolerant *Populus tremuloides*, accounting for competition increased the correlation between $\tilde{\rho}_0$ and P_{occ}, whereas the correlations for the non-boreal shade-tolerant species (*Acer rubrum*, *Acer saccharum*, *Betula alleghaniensis*, *Fagus grandifolia*, *Pinus strobus* and *Tsuga canadensis*) were similar with and without competition (Figure 6). Species distribution models that were based on random forests accurately described occurrence probabilities for all species (R^2_{Tjur} ranging from 0.74 to 0.85).

4 | DISCUSSION

We developed a model to investigate how climate and competition determine continental-scale variation in tree demography. We modelled variation in radial growth and mortality and, when combined with values for the effective fecundity from the literature, we derived the population growth rate, R_0, for size-structured populations. We redescribed R_0 as ρ_0 when using the fecundity function of Purves et al. (2008) and scaled it accordingly (i.e., $\tilde{\rho}_0$) to emphasise spatial variation in demography under constant fecundity. We then correlated $\tilde{\rho}_0$ with occurrence probabilities where competition was absent or present and found marked variation among species and competition levels, which ranged from negative to positive. Our method advances previous analyses of ontogenic growth (McGill, 2012; Thuiller et al., 2014) by including explicit representations of the complex history of forest stands (i.e., tree cohorts), the abiotic environment and species interactions. These three mechanisms commonly shape species responses to climate change, together with dispersal, evolution and physiology (Urban et al., 2016). Nonetheless, adding demography, environment and species interactions for size-structured population models comes with trade-offs: more detailed models are data intensive and might require specific information, while increasing the complexity of parameter estimations. Our approach was computationally challenging, given that it combined 3,816,854 tree measurements with climate data and competition (computed using 7,704,442 measurements). Finally, we tested whether species performance declines towards species range limits, while accounting for competition and found no support for this hypothesis for most species. Overall, our results demonstrate an extreme variability in growth and mortality rates and the difficulties that relate tree demography to species distributions.

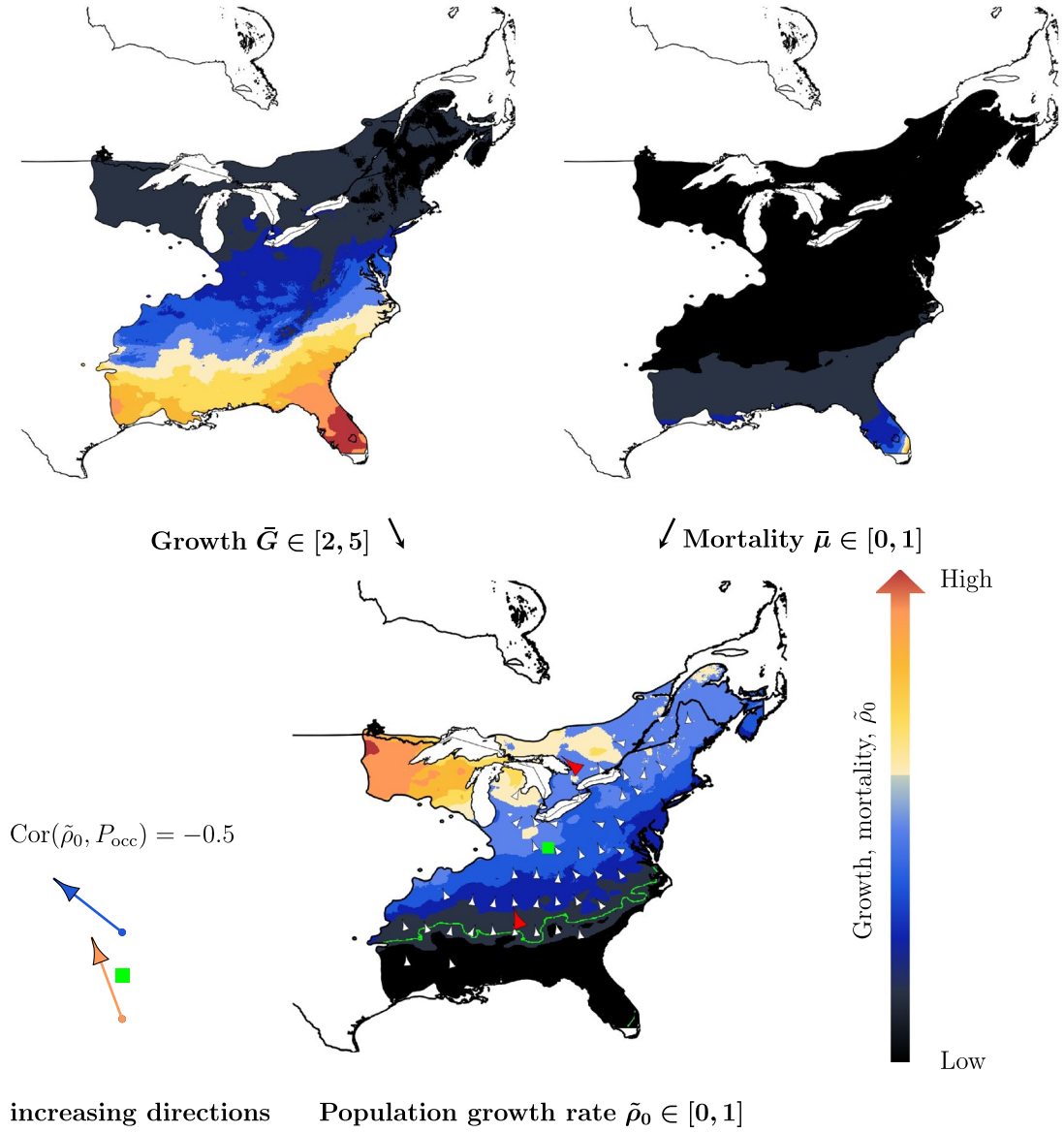

FIGURE 4 Example results for *Acer rubrum*, with a canopy height $s_c^* = 10$ m, and with 2006–2010 climate data. Population growth rate, $\tilde{\rho}_0$, results from G, μ (averaged on the maps) and constant fecundity. For many species, including *Acer rubrum*, $\tilde{\rho}_0$ does not increase towards the centre of the distribution (green square). If the abundant-centre hypothesis were validated, then the red arrows on the map (or equivalently, the blue and orange arrows on the left-hand side) would point towards the green square. These two arrows are the respective northern and southern averages of the vector field, $\nabla\tilde{\rho}_0$, that is depicted by the white arrows on the map of $\tilde{\rho}_0$. The correlation between $\tilde{\rho}_0$ and the probability of occurrence, P_{occ}, is −0.5, which is the smallest correlation for all species. Overall, we found no rule relating probabilities of occurrence to demography (see Figure 6). The green line delimits the range of *Acer rubrum* (see Supporting Information Appendix S5, Table S5.3)

4.1 | From climate to occurrence through demography

4.1.1 | Effect of climate on radial growth and mortality

Both individual growth and mortality were highly variable along the broad investigated climatic gradient. There is a long tradition in dendrochonological studies (e.g., Aussenac et al., 2017) of relating variation in the annual growth of individual trees to interannual variation in climate. Yet, it appears that the effect of climate on demography is more difficult to detect when comparing the average performance of individual trees across a large biogeographical area, especially when we integrate growth and mortality over the entire life cycle of a forest stand. Many other factors might condition forest dynamics beyond the effect of climate (Zhang et al., 2015). Tree demography is likely to be a high-dimensional process (Clark, et al., 2011) that is affected by several individual level constraints,

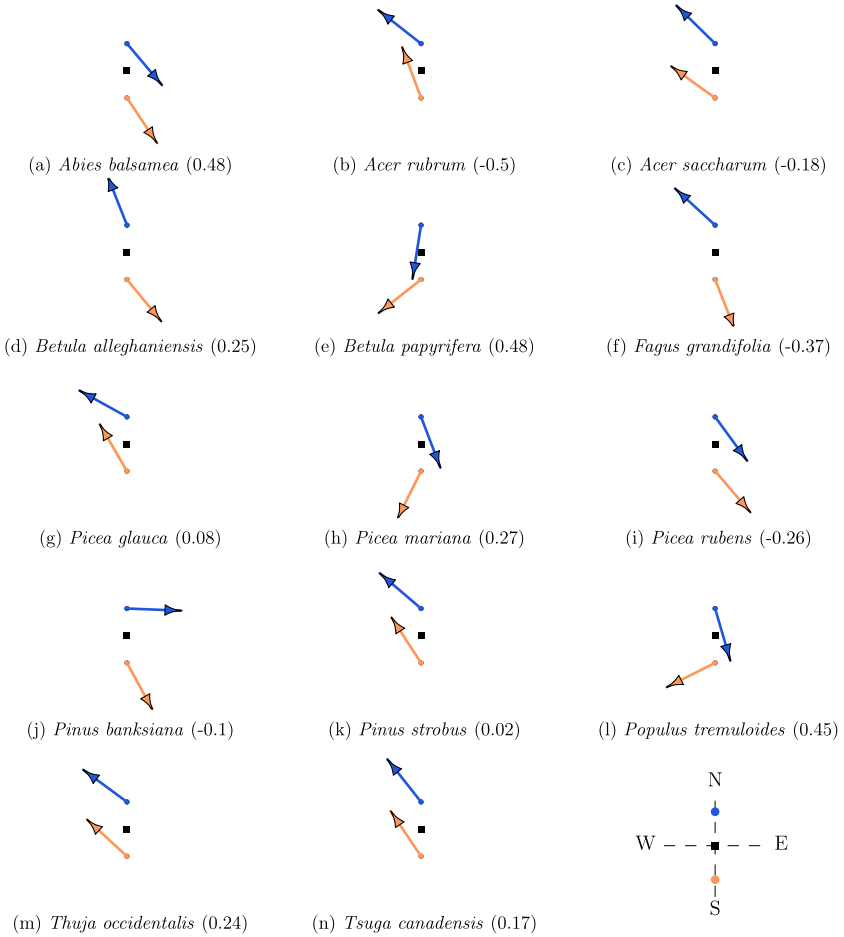

FIGURE 5 Species-specific averaged direction of increase in population growth rate, $\tilde{\rho}_0$, for the northern region (blue arrows) and southern region (orange arrows). The black square represents the species-specific centroid of the distribution, Ω, and is the reference point that defines the northern region (everything north of the centroid) and the southern region. If population performances were higher in the centre of the distribution, then the arrows would point towards the centroid. The number within parentheses is the correlation between $\tilde{\rho}_0$ ($s^* = 10$ m) and the random forest. See Figure 6 and the Supporting Information Appendix S6 for the correlations, and the Supporting Information Appendix S5, Figure S5.33 for the azimuths

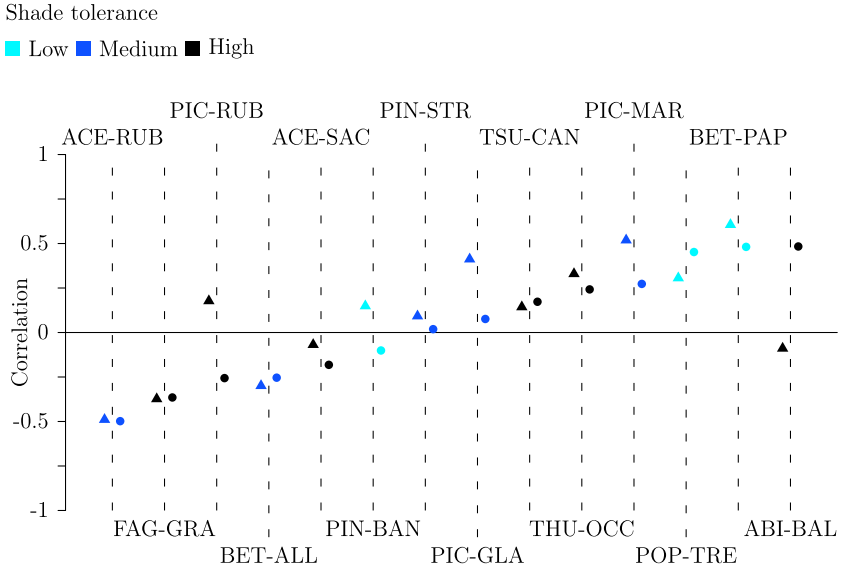

FIGURE 6 Species-specific correlations of population growth rate, $\tilde{\rho}_0$, and the species distribution model without competition (filled triangles) or with competition (canopy height $s^* = 10$ m, filled circles). The species' codes can be found in Supporting Information Appendix S2, Table S2.1. The three colours correspond to the shade tolerance level (the darker the colour, the more shade tolerant). The values can be found in Supporting Information (Appendix S6). In this figure, we sorted the data by increasing order of correlation with competition (filled circles) rather than alphabetical order

such as genetics, soil properties, microtopography, forest composition, pests, and tree and stand history. Tree mortality is also a slow and cumulative process that might be difficult to represent with discrete information, such as stem diameter, average climate and neighbourhood composition. Models such as the ones that we investigated could not properly account for external causes of death, such as physical damage (Larson & Franklin, 2010, uprooting, stem breakage, crushing by other falling trees) or dieback. Our observations that plot random effects are large relative to the effects of climatic variables is good evidence that this individual/site level variation is driving much of the uncertainty in tree demography across the climatic gradient. Including all these extra variables in growth and

mortality models (provided we have proper information and functions to represent their effects) would certainly aid in reducing the uncertainty in the functions that relate demography to climate. That being said, individual conditions, such as past history and microsite properties, are highly variable and unpredictable in nature. This means that even though we could improve further growth and mortality models by trimming residual variation, the uncertainty in some of the conditioning variables would propagate and still make demography highly variable across climatic gradients. In other words, the stochastic variation in individual conditions is simply overwhelming the deterministic effect that climate alone exerts on growth and mortality, thereby precluding any significant effect of demography on species distributions.

4.1.2 | Effect of competition on radial growth and mortality

Despite the substantial variability that we observed, we found that radial growth and mortality are strongly influenced by asymmetrical competition for light. We have found a relationship between shade tolerance and the effect of light competition for both growth (G) and mortality (μ). It suggests that not only understorey tree survival, but also understorey tree growth could help to quantify tree species competitive ability, although this analysis should be approached with caution (Feng et al., 2018). Notwithstanding that the response of growth to climate is mediated by the canopy status, we did not explore further the interaction between climate and light competition for our 14 species. We already know that the growth response of these species to adverse climate conditions is buffered by neighbourhood interspecific competition (Aussenac et al., 2019). Understanding the effect that light competition plays in tree demography is, therefore, of primary importance and requires dedicated studies, given that light and water availability act nonlinearly on plant performance (Holmgren et al., 2012). The dominance of size and competition effects over climate in our models demonstrates the importance of considering population structure in forest dynamics. Our derivation of an integrated measure of performance across the life cycle is needed to investigate the variation in demography across large areas properly.

Our two-state canopy model cannot compare with a 10-layer model as proposed by Lischke et al. (1998), which might explain why competition had little effect on correlations between probabilities of occurrence and species performance. However, two layers were sufficient to detect a joint effect of climate and competition for light on species distributions. In the absence of competition, we found that every species exhibited positive population growth rates across most of their ranges (Supporting Information Appendix S5, Table S5.3). When adding competition (canopy height $s_c^* = 10$ m), boreal species showed a substantial reduction in the proportion of the range with positive growth, from 0.01% (*Thuja occidentalis*) to 99% (*Pinus banksiana*). It is possible that we underestimated $\tilde{\rho}_0$ in northern locations because we had set a standard canopy height of 10 m across regions, and we did not consider variation in the allometric relationships that we used. Among the other species, *Populus tremuloides* lost 66% of suitable locations within its range, Ω, with the addition of competition, whereas *Acer rubrum* lost 28% (see Supporting Information Appendix S5). *Populus tremuloides* is classified as very shade intolerant (Burns & Honkala, 1990b); thus, declines in its growth owing to competition could be expected, because recruitment does not occur continuously in the understorey. We did not include disturbances in our model, but these might play a major role in maintaining this pioneer species in Eastern Canada (Nlungu-Kweta et al., 2017). Population growth rates were positive for all the other species within their distributions, regardless of the presence or absence of competition. This response supports previous studies showing that the geographical distributions (Ω) of species are within their ecological niches (Lee-Yaw et al., 2016; Csergo et al., 2017).

4.1.3 | Relationship between demography and distribution

The net reproduction rate, ρ_0 (and equivalently, $\tilde{\rho}_0$), is a heuristic tool to summarise how individual growth, mortality and seed production, which collectively define species persistence. We found four drivers that we can alter to change ρ_0: the competition, the average understorey growth, the average mortality rate and the fecundity function. The combination of these four drivers can represent the growth–survival trade-off (e.g., the ratio of mortality over radial growth μG appearing in Equation 12) and the stature–recruitment trade-off (which distinguishes long-lived pioneers from short-lived breeders). These two trade-offs are important for understanding forest dynamics (Rüger et al., 2020, for tropical forest).

We found little support for the hypothesis that tree species should be distributed where they perform the best. There were very low positive correlations between $\tilde{\rho}_0$ and occurrence probabilities. We compared the effects of using random forests rather than presence/absence data, but found no difference in the trends (Supporting Information Appendix S6). Given the high R^2_{Tjur}, we cannot attribute the lack of correlation to the random forest algorithm used to smooth the occurrence probabilities for the different tree species across their distributions. Our study adds to a growing body of literature on this subject (Holt, 2020, and references therein). For instance, a similar lack of correlation has been found for European trees (Csergo et al., 2017, using matrix projection models) and for western North American species along moisture gradients (Bohner & Diez, 2019). Local interactions are hypothesised to preclude species distribution models from predicting population growth rates when fitted to macroclimate data (Csergo et al., 2017). Although competition for light is important, our results show that there might be other mechanisms underlying abundance or population growth rates. For example, certain species have undergone negative density dependence (Yenni et al., 2012, for rare species), whereas certain common

species are limited by plant–soil feedbacks (Solarik et al., 2020, *Acer saccharum*).

Competition influenced correlations of the population growth rate, $\tilde{\rho}_0$, with the probability of occurrence (P_{occ}) and with distance to the closest edge (Figure 6; Supporting Information Appendix S6). For all the boreal species, except for *Abies balsamea*, competition attenuated the signal between P_{occ} and $\tilde{\rho}_0$ by reducing the correlation to a value closer to zero. As previously discussed, a canopy height of 10 m might be too great in comparison to what is generally found beyond a certain latitude. For the same reason, the correlations between $\tilde{\rho}_0$ and the distance to the closest edge might have been masked by competition. For *Betula papyrifera*, *Picea mariana* and *Thuja occidentalis*, for example, we found support for declining performance towards species range edges, but exclusively in open canopies. Thus, competition might have an important role at the northern border of certain species through its influence on demography. The effects of competition at range edges have recently been investigated for European trees, with a different outcome: competition was a strong determinant of vital rates, but its effect was not stronger at the edge than at the centre of the distribution (Kunstler et al., 2020). Despite this response, the authors also found a weak support for declining performance at the range edge (the abundant-centre hypothesis). For most species, we found that $\tilde{\rho}_0$ increased monotonically towards their northern or southern boundaries but not towards their centres (Figure 5; Supporting Information Appendix S5, Figure S5.33).

4.2 | Tree demography beyond growth and mortality

4.2.1 | Fecundity

It is difficult to cover the full range of the life cycle of a tree and study its specific relationships with climate. Our model does not account for spatial variability in seed production, seed survival or germination, for which very little is known and documented. We used $\tilde{\rho}_0$ instead of ρ_0 to tease apart the fecundity term. This measure can be compared directly between species to observe trends in population performance within a landscape when species fecundities are kept constant. Although the threshold value allowing species persistence is always one when using the unscaled population growth rate, ρ_0, it becomes species specific when using $\tilde{\rho}_0$. Our study also overlooked seedling growth and survival because no data are available for individual trees below a certain diameter. The ensemble of processes, from seed to seedling survival, describes the recruitment niche, which defines the requirements that allow a seed to germinate and establish (Valdez et al., 2019). Different studies that focus upon a single species (Solarik et al., 2016, *Acer saccharum*), or along either a longitudinal gradient (Clark et al., 2011) or a latitudinal gradient (Boisvert-Marsh et al., 2019), provide good evidence of the role that climate plays in shaping the recruitment niche. More specifically, seed production, rather than tree growth and mortality, was found to be the most responsive to spring temperature and summer drought (Clark et al., 2011, sites in the Appalachians and Piedmont of North Carolina). Soil properties and pathogens were found to constrain the regeneration of trees even more strongly than did climate (Brown & Vellend, 2014, Mont Mégantic, Québec). These studies corroborate the plethora of mechanisms underlying population growth rates and underscore our need for more data on the juvenile stage, at least to avoid extrapolating demographic rates that have been estimated mostly from adult trees (d.b.h. ≥ 100 mm) to saplings. A sensitivity analysis of $\tilde{\rho}_0$ with respect to the three vital rates is necessary to make further progress and to distinguish which demographic parameter is the most important in the context of climate change, and for which species, at which stage and in which part of the range.

4.2.2 | Dispersal

We posed the hypothesis of local dispersal, using a Dirac distribution (i.e., the dispersion does not appear in our equation) for the sake of tractability. Therefore, $\tilde{\rho}_0$ is a quantity derived only from demographic processes, neglecting potential effects of source and sink dynamics on distribution. The role of dispersal in tree distribution is controversial. Certain studies have reported that long-distance dispersal determines the migration rate of trees and can explain some species shifts (Nathan et al., 2002, and references therein), whereas other studies have argued that microrefugia (small patches beyond the main distribution) play a major role in colonisation (Feurdean et al., 2013, and references therein). These hypotheses could be investigated numerically with our model by developing an algorithm adapted to transport equations, such as Equation 1. However, retrieving analytical results would require simpler radial growth and mortality functions.

4.3 | Looking forward

Although ρ_0 has useful theoretical properties (Supporting Information Appendix S1), it is too early to use it in assisted migration debates and forest management. Nevertheless, we note that some species exhibited low values of ρ_0 in the southern portion of their distribution, but increased moving northwards, which might be a sign of future mismatches between their niches and their distributions. This is particularly true for *Acer rubrum*, which is projected to have extinction debts in the south (Talluto et al., 2017). Species that are poorly dispersed and highly persistent might be more subject to niche-distribution mismatches (Pagel et al., 2020, on shrubs, not trees, in the family Proteaceae in South Africa). It is, therefore, important to discern which scale is the best to understand how tree distributions emerge from forest dynamics.

Tree demography is a multidimensional process resulting from the characteristics of individual (e.g., genetics, history, size) and from local conditions that are entangled with regional processes. One way to acknowledge our incomplete understanding or the high degree of variability in demography is to use stochasticity in modelling

processes, at the cost of losing the analytical population growth rate. Integral projection models (IPMs) are stage- or size-structured models, like ours, and are promising tools to model forest dynamics (Kunstler et al., 2020; Merow et al., 2014; Vindenes et al., 2012). IPMs can integrate stochasticity into demography, which is a major feature, because chance plays a significant role in lifetime reproductive success variance and, by extension, in the variance of R_0 (Snyder & Ellner, 2016, 2018).

4.4 | Conclusion

Our study stresses that using climate through demographic rates is not enough to explain species distributions, although we accounted for forest structure and competition for light via a simplified method. Therefore, climatic niche should be used in circumspect manner, because the underlying processes of species occurrence remain unclear. We demonstrated that climate plays either a minor role or an unpredictable role in tree demography. Hence, other factors, such as stochastic extinction, dispersal limitation, sink populations or Allee effects (Holt & Keitt, 2005, and references therein), should be investigated to understand tree range dynamics. We also showed that individual processes (according to the manner in which we estimated them) contributed very little to tree distributions. Therefore, tree dynamics cannot rely exclusively upon demographic rates that are determined by local spatial processes; they should also include phenomena that can be perceived mostly at the meta-population scale, such as fire dynamics. Our study underlines the need to mix scales and to use integrated population modelling (Isaac et al., 2020).

ACKNOWLEDGMENTS

This research was enabled, in part, by support provided by Calcul Québec (http://www.calculquebec.ca/en/) and Compute Canada (www.computecanada.ca). This research was funded by a Strategic Grant from the Natural Sciences and Engineering Research Council of Canada. The authors are grateful to F. Guillaume Blanchet for helpful discussions and to William F. J. Parsons for polishing the English language.

DATA AVAILABILITY STATEMENT

All scripts that were used in this study and the trace plots of the Markov chains can be found on Github (https://github.com/amael-ls/code_R0niche). Most of the figures were made using the package *tikzDevice*. The data that support the findings of this study are available from the Forest Inventory and Analysis (FIA, USDA Forest Servive), Ministère des Forêts, de la Faune et des Parcs du Québec (MFFPQ), the Ministry of Natural Resources and Forestry of Ontario (MNRFO), the Ministry of Natural Resources of New Brunswick, and the forest products company Domtar. Restrictions apply to the availability of these data, except for FIA, which were used under license for this study. FIA data are available from https://www.fia.fs.fed.us/. Data from MFFPQ, MNRFO, the Ministry of Natural Resources of New Brunswick and Domtar can be requested from their platforms (Sharpsteen & Bracken, 2020).

ORCID

Amaël Le Squin https://orcid.org/0000-0003-3516-4155
Isabelle Boulangeat https://orcid.org/0000-0002-8463-7046
Dominique Gravel https://orcid.org/0000-0002-4498-7076

REFERENCES

Aussenac, R., Bergeron, Y., Ghotsa Mekontchou, C., Gravel, D., Pilch, K., & Drobyshev, I. (2017). Intraspecific variability in growth response to environmental fluctuations modulates the stabilizing effect of species diversity on forest growth. *Journal of Ecology*, *105*, 1010–1020. https://doi.org/10.1111/1365-2745.12728

Aussenac, R., Bergeron, Y., Gravel, D., & Drobyshev, I. (2019). Interactions among trees: A key element in the stabilising effect of species diversity on forest growth. *Functional Ecology*, *33*, 360–367. https://doi.org/10.1111/1365-2435.13257

Barton, K. (2019). Mumin: Multi-model inference. R package version 1.43.6. https://CRAN.R-project.org/package=MuMIn

Bates, D., Mächler, M., Bolker, B., & Walker, S. (2015). Fitting linear mixed-effects models using lme4. *Journal of Statistical Software*, *67*(1), 1–48. https://doi.org/10.18637/jss.v067.i01

Bohner, T., & Diez, J. (2019). Extensive mismatches between species distributions and performance and their relationship to functional traits. *Ecology Letters*, *23*, 33–44. https://doi.org/10.1111/ele.13396

Boisvert-Marsh, L., Périé, C., & de Blois, S. (2019). Divergent responses to climate change and disturbance drive recruitment patterns underlying latitudinal shifts of tree species. *Journal of Ecology*, *107*, 1956–1969. https://doi.org/10.1111/1365-2745.13149

Brown, C. D., & Vellend, M. (2014). Non-climatic constraints on upper elevational plant range expansion under climate change. *Proceedings of the Royal Society B: Biological Sciences*, *281*, 20141779. https://doi.org/10.1098/rspb.2014.1779

Brown, J. H., Gillooly, J. F., Allen, A. P., Savage, V. M., & West, G. B. (2004). Toward a metabolic theory of ecology. *Ecology*, *85*, 1771–1789. https://doi.org/10.1890/03-9000

Burns, R. M., & Honkala, B. H. (1990a). Silvics of North America: Conifers. Washington, DC: U.S. Department of Agriculture, Forest Service. www.fs.usda.gov/treesearch/pubs/1547

Burns, R. M., & Honkala, B. H. (1990b). Silvics of North America: Hardwoods. Washington, DC: U.S. Department of Agriculture, Forest Service. www.fs.usda.gov/treesearch/pubs/1548

Clark, J. S. (2003). Uncertainty and variability in demography and population growth: A hierarchical approach. *Ecology*, *84*, 1370–1381. https://doi.org/10.1890/0012-9658(2003)084[1370:UAVIDA]2.0.CO;2

Clark, J. S., Bell, D. M., Hersh, M. H., Kwit, M. C., Moran, E., Salk, C., … Zhu, K. (2011). Individual scale variation, species-scale differences: Inference needed to understand diversity. *Ecology Letters*, *14*, 1273–1287. https://doi.org/10.1111/j.1461-0248.2011.01685.x

Clark, J. S., Bell, D. M., Hersh, M. H., & Nichols, L. (2011). Climate change vulnerability of forest biodiversity: Climate and competition tracking of demographic rates. *Global Change Biology*, *17*, 1834–1849. https://doi.org/10.1111/j.1365-2486.2010.02380.x

Csergo, A. M., Salguero-Gómez, R., Broennimann, O., Coutts, S. R., Guisan, A., Angert, A. L., … Buckley, Y. M. (2017). Less favourable climates constrain demographic strategies in plants. *Ecology Letters*, *20*, 969–980. https://doi.org/10.1111/ele.12794

de Roos, A. M. (1997). A gentle introduction to physiologically structured population models. In S. Tuljapurkar & H. Caswell (Eds.), *Structured-population models in marine, terrestrial, and fresh water systems* (Chap. 5, pp. 119–204). Boston, MA: Springer US. https://doi.org/10.1007/978-1-4615-5973-3_5

Diekmann, O., Heesterbeek, J., & Metz, J. (1990). On the definition and the computation of the basic reproduction ratio R_0 in models for infectious diseases in heterogeneous populations. *Journal of Mathematical Biology*, *28*, 365–382. https://doi.org/10.1007/BF00178324

Dybzinski, R., Farrior, C., Wolf, A., Reich, P. B., & Pacala, S. W. (2011). Evolutionarily stable strategy carbon allocation to foliage, wood, and fine roots in trees competing for light and nitrogen: An analytically tractable, individual-based model and quantitative comparisons to data. *The American Naturalist*, *177*, 153–166. https://doi.org/10.1086/657992

Farrior, C. E., Dybzinski, R., Levin, S. A., & Pacala, S. W. (2013). Competition for water and light in closed-canopy forests: A tractable model of carbon allocation with implications for carbon sinks. *The American Naturalist*, *181*, 314–330. https://doi.org/10.1086/669153

Feng, J., Zhao, K., He, D., Fang, S., Lee, T., Chu, C., & He, F. (2018). Comparing shade tolerance measures of woody forest species. *PeerJ*, *6*, e5736. https://doi.org/10.7717/peerj.5736

Feurdean, A., Bhagwat, S. A., Willis, K. J., Birks, H. J. B., Lischke, H., & Hickler, T. (2013). Tree migration-rates: Narrowing the gap between inferred post-glacial rates and projected rates. *PLoS One*, *8*, e71797. https://doi.org/10.1371/journal.pone.0071797

Gelman, A., Goodrich, B., Gabry, J., & Vehtari, A. (2018). R-squared for Bayesian regression models. *The American Statistician*, *73*, 307–309. https://doi.org/10.1080/00031305.2018.1549100

Gelman, A., & Rubin, D. B. (1992). Inference from iterative simulation using multiple sequences. *Statistical Science*, *7*, 457–472. https://doi.org/10.1214/ss/1177011136

Godsoe, W., Jankowski, J., Holt, R. D., & Gravel, D. (2017). Integrating biogeography with contemporary niche theory. *Trends in Ecology and Evolution*, *33*, 159–167. https://doi.org/10.1016/j.tree.2017.03.008

Goodrich, B., Gabry, J., Ali, I., & Brilleman, S. (2018). Rstanarm: Bayesian applied regression modeling via Stan. R package version 2.17.4. http://mc-stan.org/

Gray, A., Brandeis, T., Shaw, J., McWilliams, W., & Miles, P. (2012). Forest inventory and analysis database of the United States of America (FIA). *Biodiversity & Ecology*, *4*, 225–231. https://doi.org/10.7809/be.00079

Holmgren, M., Gómez-Aparicio, L., Quero, J. L., & Valladares, F. (2012). Non-linear effects of drought under shade: Reconciling physiological and ecological models in plant communities. *Oecologia*, *169*, 293–305. https://doi.org/10.1007/s00442-011-2196-5

Holt, R. D. (2009). Bringing the Hutchinsonian niche into the 21st century: Ecological and evolutionary perspectives. *Proceedings of the National Academy of Sciences USA*, *106*(Suppl 2), 19659–19665. https://doi.org/10.1073/pnas.0905137106

Holt, R. D. (2020). Reflections on niches and numbers. *Ecography*, *43*, 387–390. https://doi.org/10.1111/ecog.04828

Holt,R.D.,&Keitt,T.H.(2005).Species'borders:Aunifyingthemeinecology. *Oikos*, *108*, 3–6. https://doi.org/10.1111/j.0030-1299.2005.13145.x

Hooten, M. B., & Hobbs, N. T. (2015). A guide to Bayesian model selection for ecologists. *Ecological Monographs*, *85*, 3–28. https://doi.org/10.1890/14-0661.1

Hutchinson, G. E. (1957). Concluding remarks. *Cold Spring Harbor Symposia on Quantitative Biology*, *22*, 415–427. https://doi.org/10.1101/SQB.1957.022.01.039

Isaac, N. J., Jarzyna, M. A., Keil, P., Dambly, L. I., Boersch-Supan, P. H., Browning, E., … O'Hara, R. B. (2020). Data integration for large-scale models of species distributions. *Trends in Ecology and Evolution*, *35*, 56–67. https://doi.org/10.1016/j.tree.2019.08.006

Kobe, R. K. (2006). Sapling growth as a function of light and landscape-level variation in soil water and foliar nitrogen in northern Michigan. *Oecologia*, *147*, 119–133. https://doi.org/10.1007/s00442-005-0252-8

Kunstler, G., Guyennon, A., Ratcliffe, S., Rüger, N., Ruiz-Benito, P., Childs, D. Z., Dahlgren, J., Lehtonen, A., Thuiller, W., Wirth, C., Zavala, M. A., & Salguero-Gomez, R. (2020). Demographic performance of European tree species at their hot and cold climatic edges. *Journal of Ecology*. https://doi.org/10.1111/1365-2745.13533

Larson, A. J., & Franklin, J. F. (2010). The tree mortality regime in temperate old-growth coniferous forests: the role of physical damage. *Canadian Journal of Forest Research*, *40*, 2091–2103. https://doi.org/10.1139/X10-149

Lee-Yaw, J. A., Kharouba, H. M., Bontrager, M., Mahony, C., Csergo, A. M., Noreen, A. M., & Angert, A. L. (2016). A synthesis of transplant experiments and ecological niche models suggests that range limits are often niche limits. *Ecology Letters*, *19*, 710–722. https://doi.org/10.1111/ele.12604

Liaw, A., & Wiener, M. (2002). Classification and regression by randomforest. *R News*, *2*, 18–22. https://CRAN.R-project.org/doc/Rnews/

Lines, E. R., Coomes, D. A., & Purves, D. W. (2010). Influences of forest structure, climate and species composition on tree mortality across the Eastern US. *PLoS One*, *5*, e13212. https://doi.org/10.1371/journal.pone.0013212

Lischke, H., Löffler, T. J., & Fischlin, A. (1998). Aggregation of individual trees and patches in forest succession models: Capturing variability with height structured, random, spatial distributions. *Theoretical Population Biology*, *54*, 213–226. https://doi.org/10.1006/TPBI.1998.1378

Little, E. L. (1971). *Atlas of United States trees. Volume 1, Conifers and important hardwoods*. Washington, D.C: U.S. Dept. of Agriculture, Forest Service. https://doi.org/10.5962/bhl.title.130546

Maguire, B. (1973). Niche response structure and the analytical potentials of its relationship to the habitat. *The American Naturalist*, *107*, 213–246. https://doi.org/10.1086/282827

McGill, B. J. (2012). Trees are rarely most abundant where they grow best. *Journal of Plant Ecology*, *5*, 46–51. https://doi.org/10.1093/jpe/rtr036

McKenney, D. W., Hutchinson, M. F., Papadopol, P., Lawrence, K., Pedlar, J., Campbell, K., … Owen, T. (2011). Customized spatial climate models for North America. *Bulletin of the American Meteorological Society*, *92*, 1611–1622. https://doi.org/10.1175/2011BAMS3132.1

Merow, C., Latimer, A. M., Wilson, A. M., McMahon, S. M., Rebelo, A. G., & Silander, J. A. (2014). On using integral projection models to generate demographically driven predictions of species' distributions: Development and validation using sparse data. *Ecography*, *37*, 1167–1183.

Nathan, R., Katul, G. G., Horn, H. S., Thomas, S. M., Oren, R., Avissar, R., & Levin, S. A. (2002). Mechanisms of long-distance dispersal of seeds by wind. *Nature*, *418*(6896), 409–413. https://doi.org/10.1038/nature00844

Nlungu-Kweta, P., Leduc, A., & Bergeron, Y. (2017). Climate and disturbance regime effects on aspen (*Populus tremuloides* Michx.) stand structure and composition along an east–west transect in Canada's boreal forest. *Forestry*, *90*, 70–81. https://doi.org/10.1093/forestry/cpw026

Olver, P. J. (2014). Linear and nonlinear waves. In *Introduction to partial differential equations* (Chap. 2, pp. 15–62). Cham: Springer International Publishing. https://doi.org/10.1007/978-3-319-02099-0_2

Pacala, S. W., Canham, C. D., Saponara, J. A. S., Jr., Kobe, R. K., & Ribbens, E. (1996). Forest models defined by field measurements: Estimation, error analysis and dynamics. *Ecological Monographs*, *66*, 1–43. https://doi.org/10.2307/2963479

Pacala, S. W., Canham, C. D., & Silander, J. A., Jr. (1993). Forest models defined by field measurements: I. The design of a northeastern forest simulator. *Canadian Journal of Forest Research*, *23*, 1980–1988. https://doi.org/10.1139/x93-249

Pagel, J., & Schurr, F. M. (2012). Forecasting species ranges by statistical estimation of ecological niches and spatial population

dynamics. *Global Ecology and Biogeography*, *21*, 293–304. https://doi.org/10.1111/j.1466-8238.2011.00663.x

Pagel, J., Treurnicht, M., Bond, W. J., Kraaij, T., Nottebrock, H., Schutte-Vlok, A. L., … Schurr, F. M. (2020). Mismatches between demographic niches and geographic distributions are strongest in poorly dispersed and highly persistent plant species. *Proceedings of the National Academy of Sciences USA*, *117*, 3663–3669. https://doi.org/10.1073/pnas.1908684117

Prasad, A. M., & Iverson, L. R. (2003). Little's range and FIA importance value database for 135 eastern US tree species. http://www.fs.fed.us/ne/delaware/4153/global/littlefia/index.html

Prasad, A. M., Iverson, L. R., & Liaw, A. (2006). Newer classification and regression tree techniques: Bagging and random forests for ecological prediction. *Ecosystems*, *9*, 181–199. https://doi.org/10.1007/s10021-005-0054-1

Pulliam, H. R. (2000). On the relationship between niche and distribution. *Ecology Letters*, *3*, 349–361. https://doi.org/10.1046/j.1461-0248.2000.00143.x

Purves, D. W. (2009). The demography of range boundaries versus range cores in eastern US tree species. *Proceedings of the Royal Society B: Biological Sciences*, *276*(1661), 1477–1484. https://doi.org/10.1098/rspb.2008.1241

Purves, D. W., Lichstein, J. W., & Pacala, S. W. (2007). Crown plasticity and competition for canopy space: A new spatially implicit model parameterized for 250 North American tree species. *PLoS One*, *2*, e870. https://doi.org/10.1371/journal.pone.0000870

Purves, D. W., Lichstein, J. W., Strigul, N., & Pacala, S. W. (2008). Predicting and understanding forest dynamics using a simple tractable model. *Proceedings of the National Academy of Sciences USA*, *105*, 17018–17022. https://doi.org/10.1073/pnas.0807754105

Ritter, P. (1987). A vector-based slope and aspect generation algorithm. *Photogrammetric Engineering and Remote Sensing*, *53*, 1109–1111.

Rüger, N., Condit, R., Dent, D. H., DeWalt, S. J., Hubbell, S. P., Lichstein, J. W., … Farrior, C. E. (2020). Demographic trade-offs predict tropical forest dynamics. *Science*, *368*(6487), 165–168. https://doi.org/10.1126/SCIENCE.AAZ4797

Sagarin, R. D., & Gaines, S. D. (2002). The 'abundant centre' distribution: To what extent is it a biogeographical rule? *Ecology Letters*, *5*, 137–147. https://doi.org/10.1046/j.1461-0248.2002.00297.x

Serrano, H. C., Antunes, C., Pinto, M. J., Máguas, C., Martins-Loução, M. A., & Branquinho, C. (2015). The ecological performance of metallophyte plants thriving in geochemical islands is explained by the Inclusive Niche Hypothesis. *Journal of Plant Ecology*, *8*, 41–50. https://doi.org/10.1093/jpe/rtu007

Sharpsteen, C., & Bracken, C. (2020). Tikzdevice: R graphics output in latex format. R package version 0.12.3.1. https://CRAN.R-project.org/package=tikzDevice

Snyder, R. E., & Ellner, S. P. (2016). We happy few: Using structured population models to identify the decisive events in the lives of exceptional individuals. *The American Naturalist*, *188*, E28–E45. https://doi.org/10.1086/686996

Snyder, R. E., & Ellner, S. P. (2018). Pluck or luck: Does trait variation or chance drive variation in lifetime reproductive success? *The American Naturalist*, *191*, E90–E107. https://doi.org/10.1086/696125

Solarik, K. A., Cazelles, K., Messier, C., Bergeron, Y., & Gravel, D. (2020). Priority effects will impede range shifts of temperate tree species into the boreal forest. *Journal of Ecology*, *108*, 1155–1173. https://doi.org/10.1111/1365-2745.13311

Solarik, K. A., Gravel, D., Ameztegui, A., Bergeron, Y., & Messier, C. (2016). Assessing tree germination resilience to global warming: A manipulative experiment using sugar maple (*Acer saccharum*). *Seed Science Research*, *26*, 153–164. https://doi.org/10.1017/S0960258516000040

Strigul, N., Pristinski, D., Purves, D. W., Dushoff, J., & Pacala, S. (2008). Scaling from trees to forests: Tractable macroscopic equations for forest dynamics. *Ecological Monographs*, *78*, 523–545. https://doi.org/10.1890/08-0082.1

Talluto, M. V., Boulangeat, I., Vissault, S., Thuiller, W., & Gravel, D. (2017). Extinction debt and colonization credit delay range shifts of eastern North American trees. *Nature Ecology & Evolution*, *1*, 0182. https://doi.org/10.1038/s41559-017-0182

Thuiller, W., Münkemüller, T., Schiffers, K. H., Georges, D., Dullinger, S., Eckhart, V. M., … Schurr, F. M. (2014). Does probability of occurrence relate to population dynamics? *Ecography*, *37*, 1155–1166. https://doi.org/10.1111/ecog.00836

Tjur, T. (2009). Coefficients of determination in logistic regression models—A new proposal: The coefficient of discrimination. *The American Statistician*, *63*, 366–372. https://doi.org/10.1198/tast.2009.08210

Urban, M. C., Bocedi, G., Hendry, A. P.,Mihoub, J.-B., Peer, G., Singer, A., … Travis, J. M. J. (2016). Improving the forecast for biodiversity under climate change. *Science*, *353*(6304), aad8466. https://doi.org/10.1126/science.aad8466

Valdez, J. W., Hartig, F., Fennel, S., & Poschlod, P. (2019). The recruitment niche predicts plant community assembly across a hydrological gradient along plowed and undisturbed transects in a former agricultural wetland. *Frontiers in Plant Science*, *10*, 88. https://doi.org/10.3389/fpls.2019.00088

Vindenes, Y., Sæther, B.-E., & Engen, S. (2012). Effects of demographic structure on key properties of stochastic density-independent population dynamics. *Theoretical Population Biology*, *82*, 253–263. https://doi.org/10.1016/J.TPB.2011.10.002

Yenni, G., Adler, P. B., & Ernest, S. K. M. (2012). Strong self-limitation promotes the persistence of rare species. *Ecology*, *93*, 456–461. https://doi.org/10.1890/11-1087.1

Zhang, J., Huang, S., & He, F. (2015). Half-century evidence from western Canada shows forest dynamics are primarily driven by competition followed by climate. *Proceedings of the National Academy of Sciences USA*, *112*, 4009–4014. https://doi.org/10.1073/pnas.1420844112

Zuur, A. F., Ieno, E. N., & Elphick, C. S. (2010). A protocol for data exploration to avoid common statistical problems. *Methods in Ecology and Evolution*, *1*, 3–14. https://doi.org/10.1111/j.2041-210X.2009.00001.x

BIOSKETCH

Amaël Le Squin is a PhD candidate, whose research interests include species distribution, niche theory and mathematical developments. His research covers one aspect of theoretical models on species distribution, community structure and ecosystem functioning currently developed by **Dominique Gravel**, principal investigator of the Integrative Ecology Lab. **Isabelle Boulangeat** currently works on species distributions and community dynamics in mountain ecosystems.

SUPPORTING INFORMATION

Additional supporting information may be found online in the Supporting Information section.

How to cite this article: Le Squin A, Boulangeat I, Gravel D. Climate-induced variation in the demography of 14 tree species is not sufficient to explain their distribution in eastern North America. *Global Ecol Biogeogr.* 2020;00:1–18. https://doi.org/10.1111/geb.13209